Growth kinetics of ellipsoidal ω-precipitates in a Ti–20 wt%Mo alloy under compressive stress

Growth kinetics of ellipsoidal ω-precipitates in a Ti–20wt%Mo alloy under compressive stress

Toru Oyama ·Chihiro Watanabe ·Ryoichi Monzen

T. Oyama[a]

[a] Division of Mechanical Science and Engineering, Graduate School of Natural Science and Technology, Kanazawa University, Kakuma-machi, Kanazawa 920-1192, Japan

E-mail: mineraru@stu.kanazawa-u.ac.jp

TEL: +81-76-234-4681

C. Watanabe[a]

[a] Division of Mechanical Science and Engineering, Graduate School of Natural Science and Technology, Kanazawa University, Kakuma-machi, Kanazawa 920-1192, Japan

E-mail: Chihiro@se.kanazawa-u.ac.jp

TEL: +81-76-234-4677

R. Monzen[a]*

[a] Division of Mechanical Science and Engineering, Graduate School of Natural Science and Technology, Kanazawa University, Kakuma-machi, Kanazawa 920-1192, Japan

TEL: +81-76-234-4678

* Corresponding author, E-mail: monzen@se.kanazawa-u.ac.jp

Abstract   The influence of applied compressive stress on the growth kinetics of ellipsoidal ω phase precipitates was investigated for a Ti–20wt%Mo alloy aged at 300 °C. The application of compressive stress accelerated the growth of ω-precipitates when the misfit strain ε_M of the precipitates along the loading direction is smaller than 0, whereas it did not essentially induce the same effect in cases where $\varepsilon_M > 0$. The growth of the precipitates was interface-controlled in the case where $\varepsilon_M < 0$ under a compressive stress of $450 - 550$ MPa. The interface-controlled growth rate increased linearly with increasing the compressive stress. The interface-controlled growth rate under a compressive stress was slower than that under the same tensile stress in the case $\varepsilon_M > 0$.

Introduction

Many investigators have examined the effects of applied external stress on the precipitation of plate-shaped second phases or disk-shaped Guinier-Preston (GP) zones in Al–Cu [1–4], Al–Zn–Mg [5], and Cu–Be [6, 7] alloys for many decades. For example, Eto et al. [2] investigated the effect of external stress on the precipitation of disk-shaped GP zones and plate-shaped θ' phase in single crystals of an Al–3.71Cu alloy (All compositions in this text are expressed by weight per cent, wt%). A tensile stress along the [001] axis during aging below 180°C assisted the preferential formation of GP zones and θ' parallel to the stress axis, and compressive stress induced the same perpendicular to the stress axis. Using a two-step aging procedure, they showed that the stress-orienting effect was initiated and determined during the nucleation stage, namely the formation of GP[I], which will grow to θ' via GP[II]. Similar stress-oriented precipitation was observed for the disk-shaped GP zones in a Cu-0.9Be single crystal [6], and the plate-shaped γ'' phase in a Cu-1.2Be-0.1Co alloy [7].

Recently, Monzen et al. [8] studied the nucleation of ω-phase precipitates in a Ti–20Mo alloy aged at 300 °C under a tensile and a compressive stress of 450 MPa. The ω-precipitates have an ellipsoidal shape slightly elongated along $<111>_\beta$ of the β-Ti matrix, with an aspect ratio of about 2. The application of tensile stress during aging the Ti–20Mo alloy accelerates the nucleation of ω-precipitates, whereas compressive stress does not essentially induce the same effect. Estimates of the average misfit strains along the loading direction and the transverse direction from measurements of the specimen length change and the lattice parameter reveal the preferential formation of specific ω-variants among four crystallographically-equivalent variants, which depends on the sense of the applied stress.

Subsequently, Monzen et al. [9] examined the effects of applied tensile stress on the growth of ellipsoidal ω-phase precipitates in a Ti–20Mo alloy aged at 300 °C. The application

of tensile stress promotes the growth of ω-precipitates when the misfit strain ε_M of the precipitates along the LD is greater than 0; however, it does not significantly affect the growth of precipitates in the case $\varepsilon_M < 0$. While the growth of precipitates under no stress or in the case $\varepsilon_M < 0$ under tensile stress is governed by the diffusion of Mo from the ω/β interface toward the β-Ti matrix, precipitate growth is instead interface-controlled in the case $\varepsilon_M > 0$ under a tensile stress of $400-550$ MPa. The growth velocity of precipitates in the case $\varepsilon_M > 0$ is proportional to the tensile stress. The activation energies for the diffusion-controlled and interface-controlled growth are estimated to be approximately 190 and 130 kJ/mol, respectively.

In this work, the growth of ellipsoidal ω-precipitates is examined for the same Ti–20Mo alloy aged at 300 °C under compressive stress. We have observed the compressive-stress-induced growth of ω-precipitates in the case $\varepsilon_M < 0$, which is in contrast with the tensile-stress-induced growth of the precipitates in the case $\varepsilon_M > 0$ [9], and further found the lower velocity of the interface-controlled growth of ω-precipitates in the case $\varepsilon_M < 0$ under a compressive stress of $450-550$ MPa than the velocity of the interface-controlled growth of ω-precipitates in the case $\varepsilon_M > 0$ under the same tensile stress, as will be shown later.

Experimental

Specimen preparation

Ti-20Mo alloy sheets were cold-rolled to a 50% reduction in thickness and then spark-cut into specimen strips. The specimens for compressive aging had a cross-section of 2 mm × 5 mm and a gage length of 7 mm. All the specimens were solution-treated at 950 °C for 2 h under vacuum and quenched in water. The solution treatment also induced complete

4

recrystallization of the specimens. The solution-treated specimens were then aged at 300 °C for 3 h under no stress (free aging). Free aging at 300 °C for 3 h induced complete nucleation of the ω-precipitates [9]. The aged specimens were further aged at 300 °C for various times under an applied compressive stress of 400, 450, 500, and 550 MPa using a creep testing device. The loading direction (LD) was parallel to the direction of the gage length. Specimens aged under a compressive stress of X MPa, a tensile stress of X MPa, and no stress are hereafter referred to as XC, XT, and 0F. The maximum applied stress of 550 MPa was approximately four-fifths the yield strength of the solution-treated specimen at 300 °C [9]. The creep strain due to dislocation motion did not essentially occur during aging at 300 °C under the maximum applied stress of 550 MPa. The lattice parameters of the solution-treated and aged specimens were measured by X-ray analysis using an X-ray diffractometer equipped with a Cu target.

Thin foils for transmission electron microscopy (TEM) observations were prepared by grinding the aged specimens from 2 mm to about 200 μm in thickness with SiC papers and by electropolishing using a solution of 60 vol% methanol, 35 vol% 2-butoxyethanol and 5 vol% perchloric acid at −20 °C and 15 V in a twin-jet electropolisher. The LDs were parallel to the broad surfaces of the TEM thin foils. TEM observations were performed using a JEOL 2010FEF microscope operated at 200 kV.

Estimate of misfit strain

As in our previous study [9], we often observed grains in which the $(113)_\beta$ plane was nearly parallel to the surfaces of TEM thin foils. The grains in which the $(113)_\beta$ plane was parallel to the specimen surfaces were used to estimate the misfit strains of the variants I and II, among the four possible ω-variants, along the LD on $(113)_\beta$ (see Fig. 1a, b in this study, and Fig. 2a,

5

b in our previous study [9]). To determine the LDs on dark-field TEM images taken using reflections due to the variants I and II, the LDs were marked on thin foils, and then the foils were carefully set in a specimen holder. The angle between the LD and the elongated $[4\bar{7}1]_\beta$ or $[\bar{7}41]_\beta$ direction of the variant I or II on $(113)_\beta$ in the grain was first measured, and the LD, i.e., $[h\ k\ l]_\beta$ and $[p\ q\ r\ s]_\omega$, was then calculated under the condition of $h^2 \le 225$, $k^2 \le 225$, $l^2 \le 225$, $p^2 \le 225$, $q^2 \le 225$, $r^2 \le 225$ and $s^2 \le 225$. The misfit strain ε_M of the variant I or II along the LD on $(113)_\beta$ was calculated using

$$\varepsilon_M = (D_\omega - D_\beta)/D_\beta, \qquad (1)$$

where D_β and D_ω are the spacings of the planes perpendicular to $[h\ k\ l]_\beta$ and $[p\ q\ r\ s]_\omega$, respectively.

Results

Relationship between size and misfit strain of ω-variants

Figure 1a, b presents dark-field TEM images of ω-precipitates in two grains in the Ti–20Mo specimens compressive-stress-aged (CSA) and tensile-stress-aged (TSA) (500 MPa) at 300 °C for 9 h after being free-aged (FA) at 300 °C for 3 h. Figure 1c is the corresponding $[113]_\beta$ selected-area diffraction pattern. The LDs of the specimens are indicated in Fig. 1a, b, since the $(113)_\beta$ plane of the grains in the specimens was nearly parallel to the specimen surfaces. Reflections due to ω-variants I and II among the four possible ω-variants were observed in Fig. 1c. The dark-field images in Fig. 1a, b were obtained using reflections due to the variant II. The variants I and II aligned with the β-Ti matrix according to the following orientation relationship: $[1\bar{1}1]_\beta$ // $[0001]_{\omega1}$; $(\bar{2}\bar{1}1)_\beta$ // $(10\bar{1}0)_{\omega1}$; $(011)_\beta$ // $(\bar{1}2\bar{1}0)_{\omega1}$ and $[\bar{1}11]_\beta$ // $[0001]_{\omega2}$; $(\bar{1}\bar{2}1)_\beta$ // $(01\bar{1}0)_{\omega2}$; $(101)_\beta$ //$(\bar{2}110)_{\omega2}$. Notably, in Fig. 1a, b, the precipitate size

6

for the variant II in the CSA specimen is larger than that for the variant II in the TSA specimen.

It may be noticed that the angles between the LD and the elongated $[4\bar{7}1]_\beta$ direction of the variant II on $(113)_\beta$ in Fig. 1a, b are almost the same, 63.5 and 64.0°, respectively. The misfit strains of the variant II along the LD in Fig. 1a, b, calculated using Eq. (1), were thus the same, -0.13. Consequently, the difference between the sizes of the ω-precipitates in Fig. 1a, b is based on the difference in the sense of the applied stress.

All four ω-variants in the specimens CSA, TSA and FA at 300 °C for various periods up to 48 h (1.728×10^5 s) had an ellipsoidal shape elongated along $<111>_\beta$, with an aspect ratio of about 2.3. Here, the shape of ω-precipitates was assumed to be a spheroid described in x-y-z coordinates by $x^2/r^2+y^2/r^2+z^2/l^2 \leq 1$, where $l \fallingdotseq 2.3r$. The diameter d of a sphere having the same volume as the ellipsoidal precipitate was then calculated. The average diameter d_0 of the ω-precipitates was 2.7 nm after the specimen was solutionized at 950 °C and then free-aged (FA) at 300 °C for 3 h [9].

The actual elongated direction of the variant II in Fig. 1a, b was along $[\bar{1}11]_\beta$. To obtain an average value of d for the variant II, the sizes of ω-precipitates of the variant along $[\bar{7}41]_\beta$ on $(113)_\beta$ were measured and then were converted into values of l along $[\bar{1}11]_\beta$ on $(011)_\beta$. The average values of r and l for the variant II in Fig. 1a, b were estimated as 3.8 and 8.7 nm, and 2.3 and 5.3 nm, respectively. About 100 precipitates were used for measurements of r and l for each. Therefore, the average values of d for the variant II were 9.8 and 5.9 nm. Similarly, we obtained average values of d for the variants I and II in the other grains in which the $(113)_\beta$ plane was parallel to the surfaces of the CSA specimens.

Figure 2 displays the growth size $d-d_0$ of variants I and II, plotted as a function of the misfit strain ε_M of precipitates along the LD for the specimens CSA (500 MPa), TSA (500 MPa) and FA at 300 °C for 9 h. The values of $d-d_0$ for the TSA specimen and the average

value ($=2.8$ nm) indicated by the solid line for the FA specimen were taken from our previous study [9]. Figure 2 shows that the values of $d-d_0$ for the CSA specimen are larger than that for the FA specimen when $\varepsilon_M < 0$, whereas they are nearly identical to that for the FA specimen when $\varepsilon_M > 0$. In contrast, the values of $d-d_0$ for the TSA specimen are larger than that for the FA specimen when $\varepsilon_M > 0$; however, they are nearly identical to that for the FA specimen when $\varepsilon_M < 0$.

The growth of the ω-variants was promoted in the specimens aged at 300 °C under a compressive stress of $400-550$ MPa in the case $\varepsilon_M < 0$; however, the compressive stress did not significantly affect the growth of the variants when $\varepsilon_M > 0$. Hereafter, ω-variants I and II in the case $\varepsilon_M < 0$ in specimens aged at 300 °C under a compressive stress of 400, 450, 500, and 550 MPa are referred to as 400CL, 450CL, 500CL and 550CL respectively, and variants in the case $\varepsilon_M > 0$ in specimens aged at 300 °C under a compressive stress of $400-550$ MPa are referred to as $400-550$CS. Similarly, variants I and II in the case $\varepsilon_M > 0$ in specimens aged at 300 °C under a tensile stress of $400-550$ MPa are referred to as $400-550$TL [9].

Growth kinetics

Figure 3a displays the growth size $d-d_0$ plotted against aging time t on logarithmic scales for ω-variants 500CL, 500CS and 500TL and for ω-variants in specimens 500C, 500T and 0F. In the initial stage of aging, a linear relationship was observed between log ($d-d_0$) and log t for all of the cases, indicating that $(d-d_0)^n$ is nearly proportional to t. In the case of 0F and 500CS, n was approximately 2; however, in the case of 500CL and 500TL, n was approximately 1. For 500C and 500T, n was between 1 and 2. Notably, the growth velocity of 500CL is slower than that of 500TL.

Figure 3b, c presents the lattice parameter a_β of the β-Ti matrix and the lattice parameters a_ω and c_ω of the ω-precipitates with a hexagonal structure as a function of t for specimens 500C, 500T and 0F. The lattice parameter of the β-Ti matrix in 500C and 500T decreases more rapidly than that in 0F and then saturates to the value of 0.3230 nm over about 165 h (5.94 ×10⁵ s), while the lattice parameters of ω-precipitates in 500C and 500T increase more rapidly than those in 0F and then saturate to the values of a_ω=0.4675 nm and c_ω=0.2836 nm over about 165 h. The saturated value of 0.3230 nm is close to the lattice parameter, 0.3229 nm, of a β-Ti solid solution containing 39wt%Mo that is the equilibrium solubility of Mo in β-Ti at 300 °C in the Ti-Mo binary phase diagram [10]. In addition, corresponding to the slower growth velocity of ω-variants in 500C than in 500T, the lattice parameter of the β-Ti matrix in 500C decreases more slowly than that in 500T, and also the lattice parameters of the ω-precipitates in 500C increase more slowly than that in 500T. Because Mo atoms, which diffuse from the ω/β interface toward the β-Ti matrix as the ω-precipitates grow [10], are smaller than Ti atoms, the increase in the concentration of Mo atoms within the β-Ti matrix and the decrease in the Mo concentration within the ω-precipitates resulted in a decrease of the β-Ti lattice parameter and increases of the lattice parameters of the ω-phase, respectively.

Figure 3d shows the number density N of ω-precipitates as a function of t for 500C, 500T and 0F. The number density is defined as the volume fraction f of precipitates divided by the average volume of a single precipitate ($N=3f/4\pi(d/2)^3$). Approximately 600 precipitates were used for estimates of d at each aging time. The volume fraction was determined by applying the lattice parameters of the β-Ti matrix in 500C, 500T and 0F in Fig. 3b to the experimental data reported for the dependence of the lattice parameter on the Mo concentration [11]. The lattice parameters of the ω-precipitates against t for 500C, 500T and

0F in Fig. 3c were also used in this calculation. In addition, the concentration of Mo in the ω-precipitates was assumed to be 10wt%, as in our previous paper [9].

In Fig. 3a, a linear relationship is seen between $\log (d-d_0)$ and $\log t$ at the stage of aging from 2 to 10 h for 500CL and 500TL, and from 2 to 165 h (5.94×10^5 s) for 0F. In the case of specimens 500C and 500T in Fig. 3d, the number density of ω-precipitates is constant from 2 to 10 h and then rapidly decreases, whereas, in the case of specimen 0F, it remains constant from 2 to 165 h. This means the growth stage of ω-precipitates from 2 to 10 h after nucleation for 500C and 500T, and from 2 to 165 h for 0F. In this stage, thus, the values of n for 500CL and 500TL, and for 0F are approximately 1 and 2.

Figure 4 shows the growth size $d-d_0$ as a function of t on logarithmic scales for 400 − 550CL. A linear relationship exists between $\log (d-d_0)$ and $\log t$ for 400 − 550CL. The values of n are calculated from the slopes of the straight lines obtained by the least-squares method. The calculated values are listed in Table 1. For 450 − 550CL, $n \doteqdot 1$. For 400 − 550CS, the values of n were approximately 2. An n-value of 2 indicates that the growth kinetics of the ω-variants follows a diffusion-controlled parabolic growth law, whereas a value of 1 indicates that the growth of the ω-variants obeys an interface-controlled growth law [12, 13]. The growth size $d–d_0$ was replotted against t for 450 − 550CL. The growth rates were obtained from the slopes of the straight lines for 450 − 550CL. The growth rate v plotted against applied stress σ is shown in Fig. 5, together with the data for 400 − 550TL [9]. The growth rate increases linearly with increasing applied compressive stress or tensile stress. Evidently, the growth rate under a compressive stress of 450-550 MPa is slower than that under the same tensile stress.

Precipitate shape

Figure 6a, b depicts dark-field TEM images of the ω-variants I and II in the same grain in the specimens CSA (500 MPa) at 300 °C for 14 days (1.21×10^6 s) after being FA at 300 °C for 3 h. The zone axis is parallel to $[113]_\beta$. Notably, the precipitate size for the variant II in Fig. 6b is larger than that for the variant I in Fig. 6a. This size difference is due to the difference in the sign of the misfit strain along the LD between the variants I and II. The misfit strains of the variants I and II along the LD in Fig. 6a, b, calculated using Eq. (1), were 0.12 and −0.19, respectively. More importantly, the variant II has an ellipsoidal shape with a smaller aspect ratio l/r than the variant I.

The average values of r and l for the variants I and II in Fig. 6a, b were estimated as 13 and 5.7 nm, and 16 and 7.8 nm, respectively. Thus, the average values of d for the variants I and II were 15 and 20 nm. The value of d ranged from 4 to 26 nm for the variant I, and from 8 and 31 nm for the variant II. The aspect ratio l/r was about 2.3 for the variant I with $d = 4 − 26$ nm, and about 2.0 for the variant II with $d = 8 − 31$ nm. Thus, the difference in the aspect ratio between the variants I and II is not based on the difference in the size between them, but the difference in the sign of the misfit strain along the LD between them.

We measured average values of d and l/r for the variants I and II in other grains in the specimen CSA (500 MPa) at 300 °C for 14 days after being FA at 300 °C for 3 h. Also we obtained average values of d and l/r in the specimen FA at 300 °C for 14 days after being FA at 300 °C for 3 h. The average d-value of 21 nm in the case of $\varepsilon_M < 0$ for all the grains examined in the CSA specimen was larger than the d-value of 13 nm for the FA specimen, whereas the average d-value of 14 nm in the case of $\varepsilon_M > 0$ was nearly identical to that for the FA specimen. The average l/r-value of 2.3 in the case of $\varepsilon_M > 0$ for the CSA specimen was identical to the l/r-value of 2.3 for the FA specimen; however, the l/r-value of 2.1 in the case of $\varepsilon_M < 0$ was smaller than that for the FA specimen.

Fratzl et al. [14] studied, by small-angle X-ray scattering, the growth of ω-precipitates in a Ti–20at%Mo (33.4wt%Mo) alloy aged at temperatures below 500 °C, and observed that the precipitate size r increases, in a first step, as $r \propto t^{1/3}$ with increasing aging time t, but then stabilizes at a constant value of r=7.5 nm. This was interpreted as a coarsening process, progressively hindered by attractive elastic interactions between ω-precipitates. The former result that the precipitate size increases as $r \propto t^{1/3}$ is in disagreement with our result that, during the growth stage of ω-precipitates in specimen 0F, the size d increases as $d \propto t^{1/2}$ with increasing t (Fig. 3a, d). However, the latter result corresponds to our result that the precipitate size for 500TL and 500CL increases very slowly over about 13 nm after the growth stage of ω-precipitates (Fig. 3a, d). Upon aging at 300 °C under a compressive and a tensile stress of 500 MPa, a coarsening stage after the growth stage of the precipitates is judged to begin over 165 h, because the lattice parameter of the β-Ti matrix and the lattice parameters of ω-precipitates in 500C and 500T decreases rapidly and increase rapidly with increasing t, respectively, and then saturate over 165 h (Fig. 3b, c).

Discussion

In our previous study [9], we have shown that (1) the application of tensile stress promotes the growth of ω-precipitates when $\varepsilon_M > 0$; however it does not significantly affect the growth of precipitates when $\varepsilon_M < 0$, and that (2) although the growth of ω precipitates under no stress or in the case $\varepsilon_M < 0$ under tensile stress is controlled by the diffusion of Mo from the ω/β interface toward the β-Ti matrix, precipitate growth is instead interface-controlled in the case $\varepsilon_M > 0$ under a tensile stress of $400-550$ MPa. In this study also, the application of compressive stress accelerates the precipitate growth; however, the growth acceleration occurs when $\varepsilon_M < 0$ (Figs. 2 and 3a). In the case $\varepsilon_M < 0$ under a compressive stress of $450-550$

MPa, the precipitate growth is interface-controlled (Fig. 4 and Table 1). Moreover, the interface-controlled-growth rate under a compressive stress of $450 - 550$ MPa is slower than the growth rate in the case $\varepsilon_M > 0$ under the same tensile stress (Fig. 5).

The origin of the results shown in Figs. $2 - 5$ can be understood to arise through the interaction energy due to the presence of misfit strains between the applied stress and the ω-precipitates, as in our previous study [9]. The interaction energy F_I per unit volume of the precipitate between an external stress σ_{ij} and a misfit strain ε_{ij} (stress-free transformation strain) is expressed as [15]

$$F_I = -\sigma_{ij}\varepsilon_{ij}. \tag{2}$$

That is, the interaction energy is the work done by the external stress during the precipitate growth. We hypothesized that the interface velocity under an external stress σ_{ij} can be expressed as [9]

$$v_I = \delta\nu[(\Delta G_m + |F_I|V_m)/RT]\exp(-\Delta G_d/RT), \tag{3}$$

where δ is the interface width, ν is the vibrational attempt frequency, ΔG_m is the difference in free energies per mol between the β- and ω-phases, V_m is the molar volume of the precipitate, R is the gas constant, T is the absolute temperature, and ΔG_d is the activation energy for interface transport.

Equations 2 and 3 predict that applied compressive stress promotes the growth of the ω-variants when $\varepsilon < 0$, but it does not affect the growth when $\varepsilon_M > 0$. This prediction is in agreement with the results shown in Figs. 2, 3a and 4. In addition, Eqs. 2 and 3 predict that the growth velocity of the precipitates in the case $\varepsilon_M < 0$ under compressive stress is slower than that of the precipitates in the case $\varepsilon_M > 0$ under tensile stress, since the average misfit strain of the ω-precipitate is estimated to be 0.010 [8]. This is the case, as shown in Fig. 5.

13

As described in the previous section, on aging at 300 °C under a compressive stress of 500 MPa, a coarsening stage after the growth stage of ω-precipitates would start over 165 h. Eq. 2 predicts that compressive stress promotes the growth of the ω-variants even in this coarsening stage when $\varepsilon_M < 0$. Eq. 2 also predicts that compressive stress does not significantly affect the growth along the elongated $<111>_\beta$ direction of the precipitates in the growth or the coarsening stage even when $\varepsilon_M < 0$, since the misfit strain of the precipitate along $<111>_\beta$ is negligibly small (−0.005~0). Accordingly the aspect ratio of the precipitates in the case of $\varepsilon_M < 0$ under compressive stress may become smaller than that of 2.3 for the precipitates in specimen 0F. However, because in the growth stage of the precipitates, concurrently Mo atoms diffuse from the ω/β interface toward the β-Ti matrix (Fig. 3b, c), the aspect ratio of 2.3 would be maintained. On the other hands, in the coarsening stage, the aspect ratio of the precipitates is expected to be smaller than 2.3, because diffusion of Mo atoms takes place among ω-precipitates. These predictions are in agreement with the results shown in Figs. 1a and 6b

Conclusions

1. Application of a compressive stress of 400 − 550 MPa during aging a Ti-20wt%Mo alloy at 300°C promotes the growth of ellipsoidal ω-precipitates when the misfit strain ε_M of the precipitates along the loading direction is smaller than 0; however it does not significantly affect the growth of the precipitates when $\varepsilon_M > 0$.

2. Compressive stress does not affect the growth kinetics when $\varepsilon_M > 0$, whereas, in the case $\varepsilon_M < 0$ under a compressive stress of 450 − 550 MPa, precipitate size increases linearly with increasing aging time. The latter observation indicates that the growth of ω-precipitates is interface-controlled.

3. The growth velocity of the precipitates in the case $\varepsilon_M < 0$ under a compressive stress of $450 - 550$ MPa is slower than that of the precipitates in the case $\varepsilon_M > 0$ under the same tensile stress [9].

Conflict of Interest: The authors declare that they have no conflict of interest.

References

1. Hosford WF, Agrawal SP (1975) Effect of stress during aging on the precipitation of θ' in Al-4 Wt pct Cu, Metall Mater Trans A 6: 87-491

2. Eto T, Sato A, Mori T (1978) Stress-oriented precipitation of G. P. Zones and θ' in an Al-Cu alloy, Acta Metall 26: 99-508

3. Skrotzki B, Shiflet G, Starke Jr EA (1996) On the effect of stress on nucleation and growth of precipitates in an Al-Cu-Mg-Ag alloy, Metall Mater Trans A 27: 431-3444

4. Zhu AW, Starke Jr EA (2001) Stress aging of Al–xCu alloys: experiments, Acta Metall 49: 285-2295

5. Chen JF, Zou LC, Chen YL, Li Q (2015) Effect of stress on precipitation behaviour of 7xxx alloy during age forming process. Mater. Sci. Technol. doi: 10.1179/1743284715Y.0000000100

6. Monzen R, Watanabe C, Seo T, Sakai T (2005) Effect of applied stress on precipitation of Guinier–Preston zones in a Cu–0.9 wt% Be single crystal, Phil Mag Lett 85: 03-612

7. Monzen R, Okawara S, Watanabe C (2012) Stress-assisted nucleation and growth of γ'' and γ' precipitates in a Cu–1.2 wt%Be–0.1 wt%Co alloy aged at 320°C, Phil Mag 92: 826-1843

8. Monzen R, Kawai R, Watanabe C (2015) Effect of external stress on nucleation of ellipsoidal ω precipitates in a Ti-20wt%Mo alloy, J Mater Sci 50: 76-1882

9. Monzen R, Kawai R, Oyama T, Watanabe C (2016) Tensile-stress-induced growth of ellipsoidal ω-precipitates in a Ti-20wt%Mo alloy, J Mater Sci 51: 2490-2498

10. Hickman BS (1969) Omega phase precipitation in alloys of titanium with transition Metals, Trans Metall Soc AIME 245: 1329-1336

11. Kun S, Xuezhong Y, Erdong W, Dongfeng C, Cheng G (2006) Neutron diffraction study

of the deuterides of Ti-Mo alloys, Physica B 385-386: 41-143

12. Christian JW (2002) The theory of in Metals and Alloys, 3rd ed., 1, Pergamon Press, Oxford

13. Aaronson HI, Enomoto M, Lee JK (2010) Mechanisms of Diffusional Phase Transformations in Metals and Alloys, CRC Press, New York

14. Fratzl P, Langmayr F, Vogl G, Miekeley W (1991) The growth of ω-phase inclusions in Ti-20at%Mo and the competition between elastic and surface energies, Acta Metall 39:753-761

15. Eshelby JD (1957) The determination of the elastic field of an ellipsoidal inclusion, and related problems, Proc R Soc A 241: 76-396

Figure and Table Captions

Fig. 1 a, b Dark-field TEM images of ω-variant II in Ti–Mo specimens compressive-stress-aged and tensile-stress-aged (500 MPa) at 300 °C for 9 h after being free-aged at 300 °C for 3 h. *LD* loading direction. **c** $[113]_\beta$ selected-area diffraction pattern corresponding to **a** and **b**

Fig. 2 Growth size $d - d_0$ for ω-variants I and II in Ti–Mo specimens compressive-stress-aged (CSA) (500 MPa), tensile-stress-aged (TSA) (500 MPa) and free-aged (FA) at 300 °C for 9 h after being FA at 300 °C for 3 h, plotted as a function of the misfit strain ε_M of ω-precipitates along the loading direction.

Fig. 3 Aging time t dependence of **a** the growth size $d - d_0$ for 500CL, 500CS and 500TL, and ω-variants in 500C, 500T and 0F, **b** the lattice parameter a_β of the β-Ti matrix in 500C, 500T and 0F, **c** the lattice parameters a_ω and c_ω of the ω-precipitates in 500C, 500T and 0F, and **d** the number density N of ω-variants in 500C, 500T and 0F. Representative error bars are shown

Fig. 4 Growth size $d - d_0$ plotted against aging time t on logarithmic scales for 400, 450, 500, and 550CL. Representative error bars are shown

Fig. 5 Applied stress σ dependence of the growth rate v for 450, 500 and 550CL, and 400, 450, 500 and 550TL. Representative error bars are shown

Fig. 6 Dark-field TEM images of ω-variants I and II in the same grain in a Ti–Mo specimen compressive-stress-aged (500 MPa) at 300 °C for 14 days after being free-aged at 300 °C for 3 h. *LD* loading direction. The zone axis is along $[113]_{\beta}$.
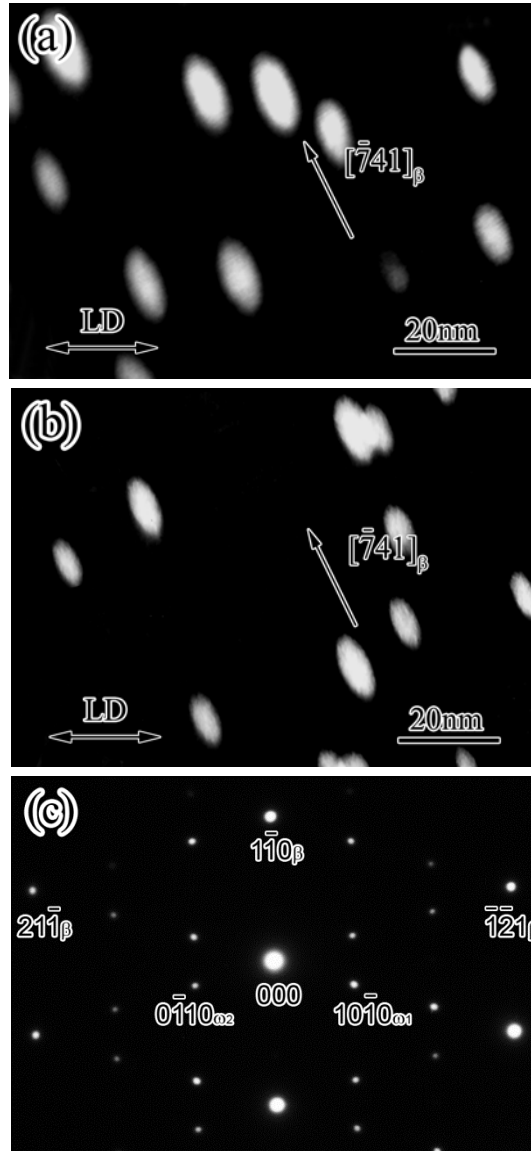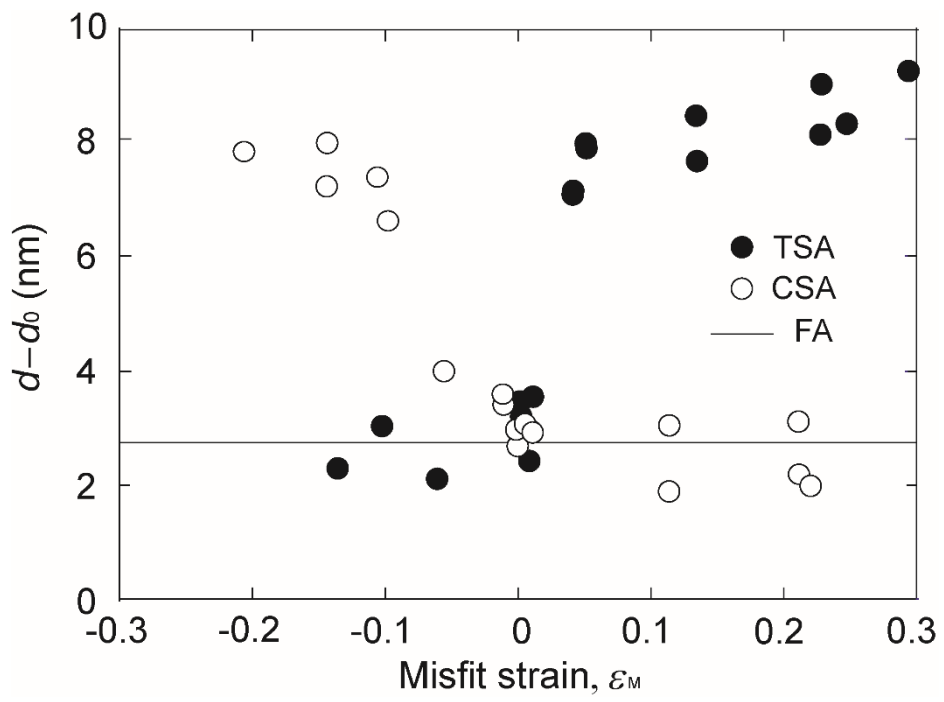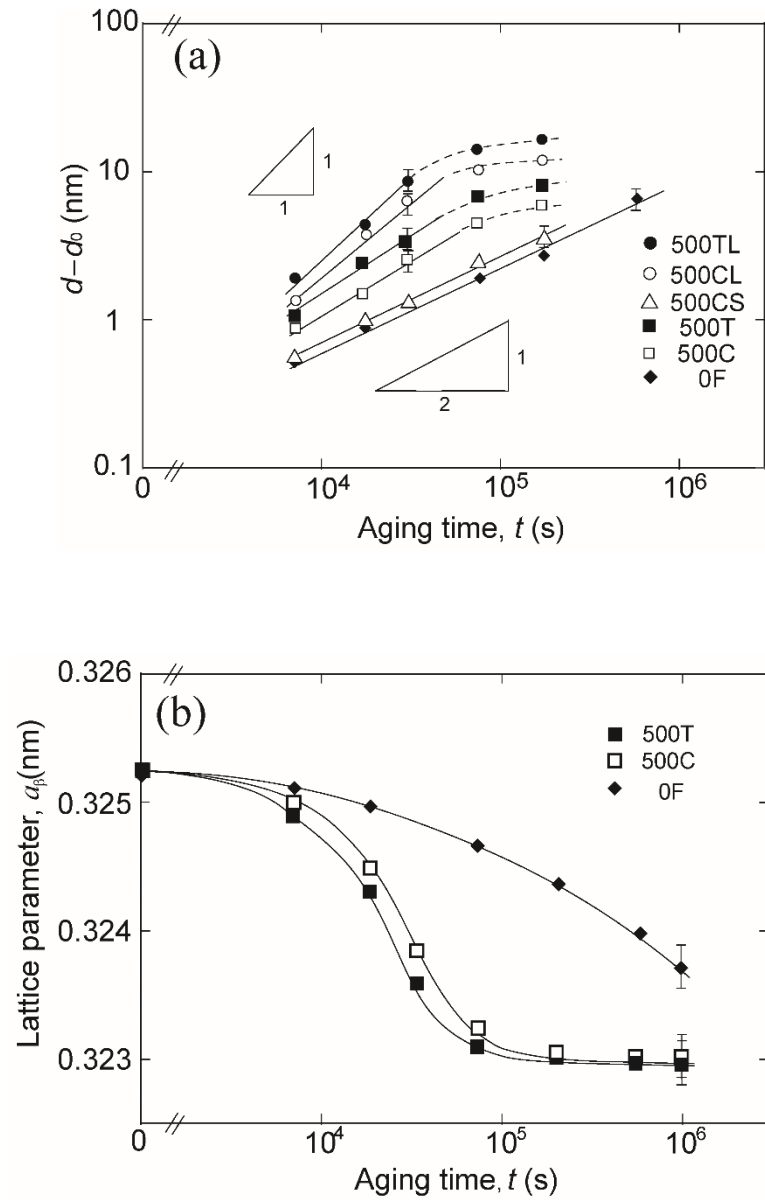
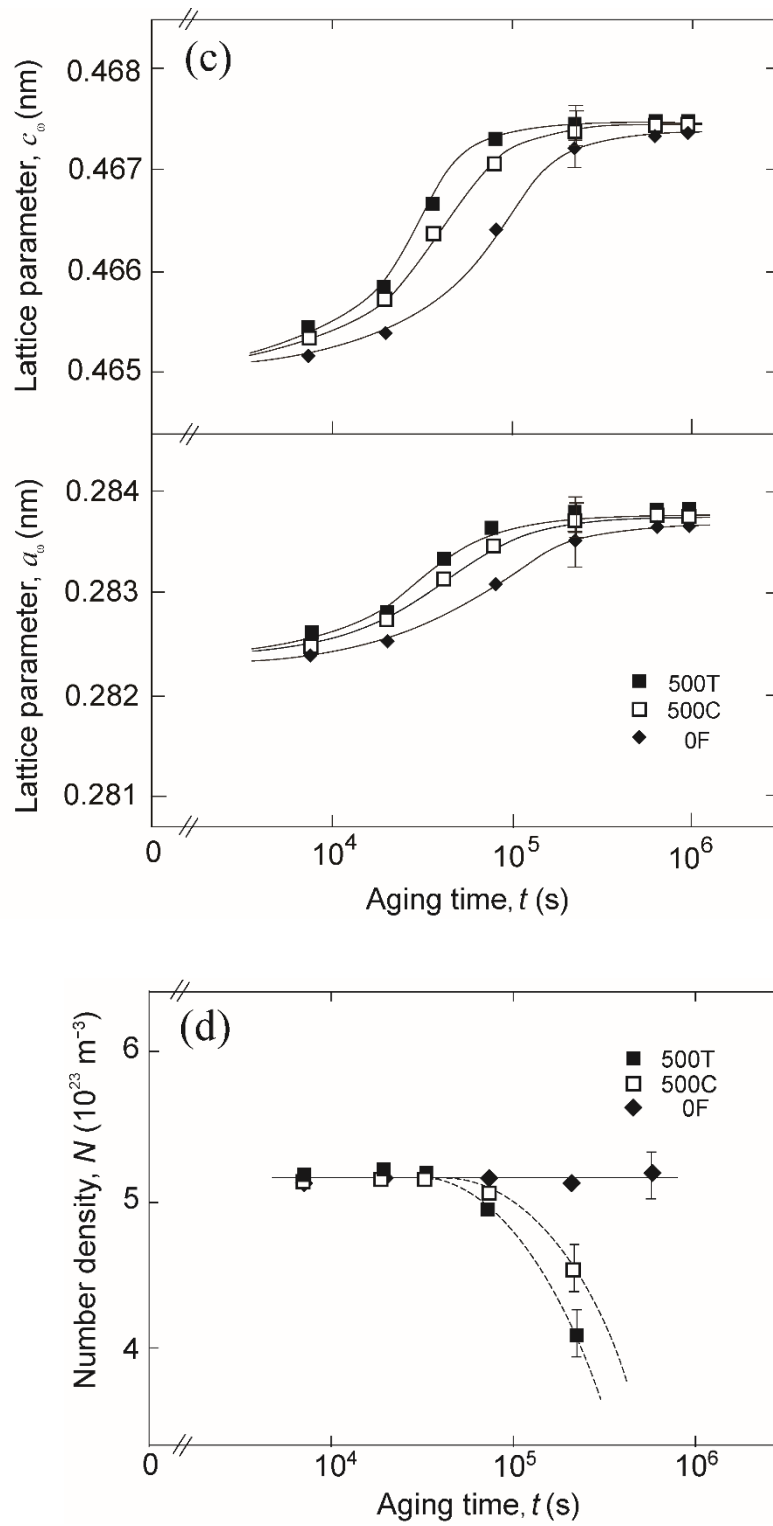**Table 1** Calculated *n* values for 400, 450, 500, and 550CL.

Fig. 1

Fig. 2

Fig. 3

Fig. 3
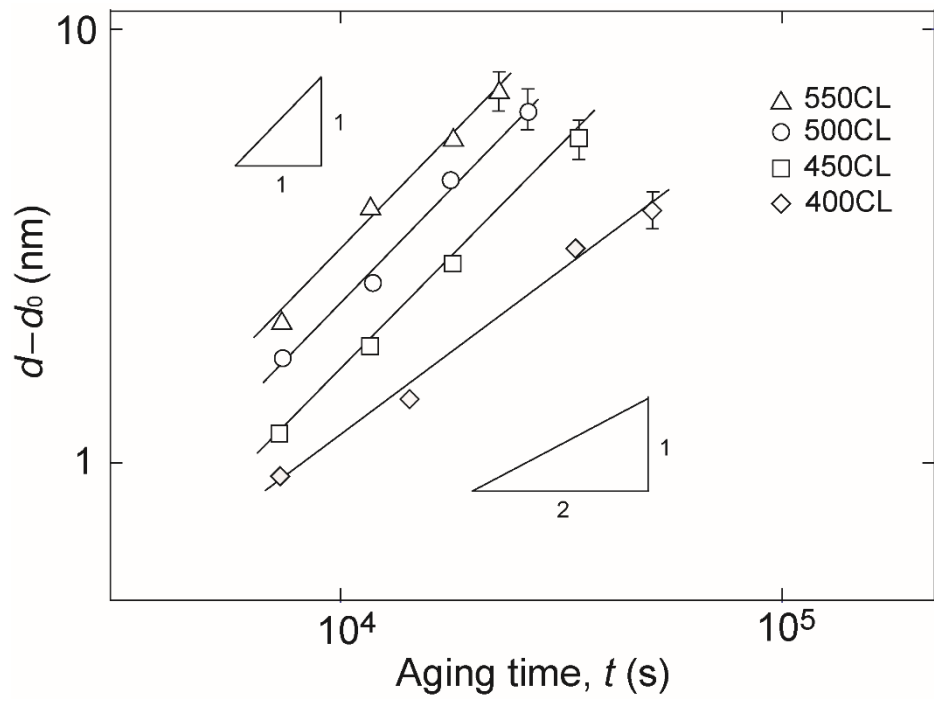
Fig. 4
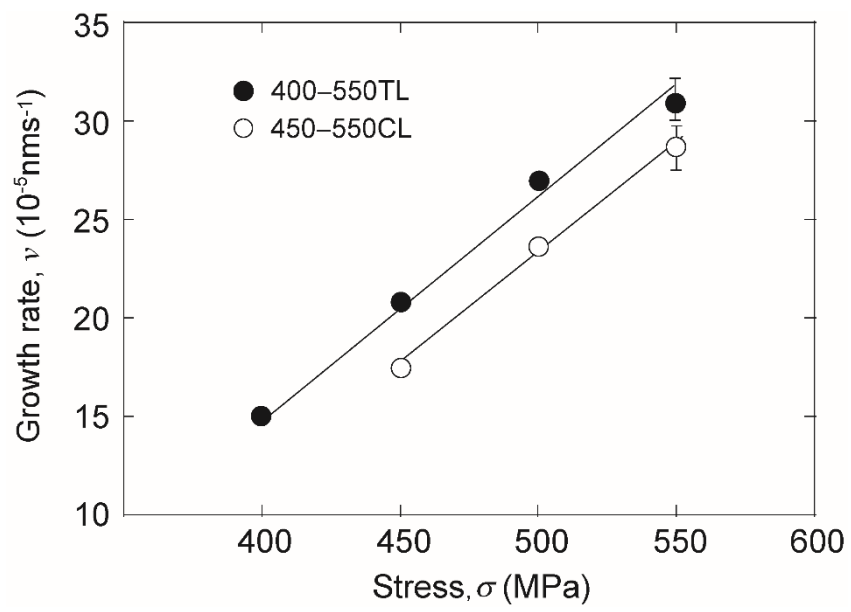
Fig. 5
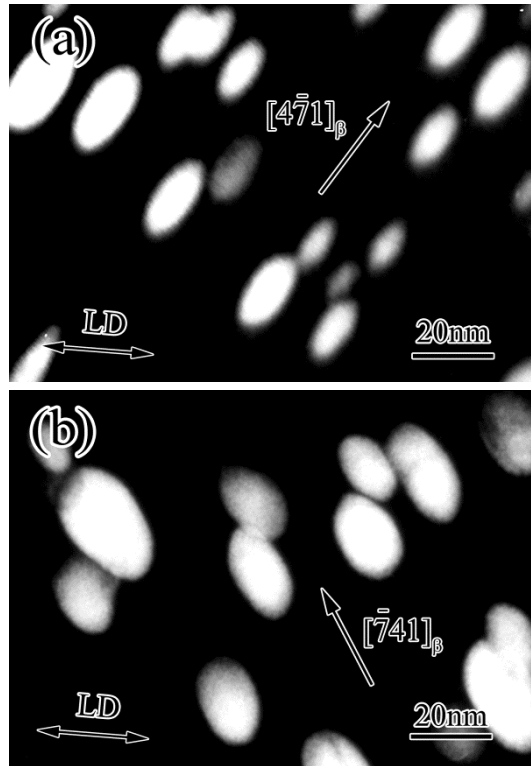
Fig. 6

Table 1

Specimen	400CL	450CL	500CL	550CL
n	1.5±0.1	1.1±0.1	1.0±0.1	1.0±0.2